Chapter VIII

In-vivo Studies

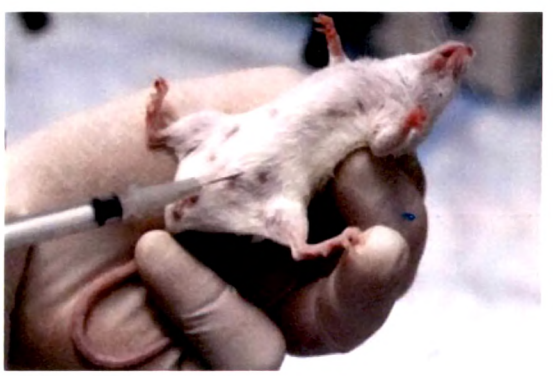

In vivo studies are prerequisite in biomedical area to confirm the efficacy of the prepared formulations with respect to their targetability as well as their capability to deliver drug specifically to the desired sites. Polymeric nanoparticles made from natural and synthetic polymers have drawn a considerable attention because of their high stability and maneuverability for industrial manufacturing, and the opportunity they offer for further surface nanoengineering. Nanoparticles can be tailor-made to achieve both controlled drug release and disease-specific localization by tuning the polymer characteristics and surface chemistry. It has been established that nano-carriers can become preferentially concentrated at infectious sites by virtue of the targeting moiety attached to them. As soon as they are accumulated at the target site, hydrophobic biodegradable polymeric nanoparticles can act as local drug depot depending upon the makeup of the carrier, providing a source for continuous supply of encapsulated therapeutic compound at the diseased site, such as solid tumor. To prolong the systemic circulation time of the nanoparticles and to enhance their passive targeting efficiency, various strategies that involve regulation of particle size and surface charge on the nanomatrices can be employed (Shenoy et al., 2005).

It is believed that the characterization of any drug carrier is incomplete without thorough investigations on its organ distribution profile. The most suitable method for investigation of *in vivo* behavior of the developed formulation is to label them with radionuclides and measure their radioactivity in various tissues and simultaneously perform gamma imaging of the whole body after administration of radiolabeled compound. For biodistribution profile

investigation of any polymeric nanocarrier system, radiolabeling of the polymer backbone is found to be the most favorable and reliable means for subsequent quantification. This chemical conjugation of the radioactive moiety is strongly dependent on the presence of reactive groups in the polymer. In this study, the formulation consisted of polymeric nanoparticles made of PLGA (RESOMER RG 503H) which have free carboxylic acid end groups. The free carboxylic end groups have the ability to react with reduced compounds to generate conjugates. Gamma ray emitting labels are usually preferred for evaluating biodistribution because of higher sensitivity and ease of sample preparation and processing. In certain cases, the bioactive compounds are labeled with beta-emitting species (like tritium) and become helpful in tracing the pathway of distribution of the pharmacologically active compound *in vivo* (Shenoy et al., 2005).

On the basis of *in vitro* characterization and stability studies, Pioglitazone solution (PIO-S), Pioglitazone dispersion (PIOD), Rosiglitazone solution (ROS-S), Pioglitazone loaded untargeted (PIO-NP) and transferrin conjugated targeted nanoparticles (Tf-PIO-NP), Rosiglitazone loaded untargeted (ROS-NP) and transferrin conjugated targeted nanoparticles (Tf-ROS-NP) were selected for *in vivo* studies for comparative evaluation.

8.1 RADIOLABELING OF FORMULATIONS

^{99m}Tc has been used to directly label preformed nanoparticles by means of stannous chloride as a reducing agent. ^{99m}Tc is cost effective, easily available and has low radiation dose (Love et al., 1989). Hence, it is extensively used for radio-labeling study. Half-life of ^{99m}Tc is 6 hrs as compared to 60 days of ^{125}I, and the absence of β-radiations permits the administration of millicurie amounts of ^{99m}Tc radio-activity without a significant radiation dose to the patient. Furthermore,

^{99m}Tc is readily available in a sterile, pyrogen-free, and carrier-free state from ^{99}Mo-^{99m}Tc generators. Reduced ^{99m}Tc is added to the nanoparticles, which easily binds to the nanoparticle's surface. This surface labeling approach is technically simple and good for the production of radiolabeled nanoparticles in a pharmaceutically acceptable form.

In the present study, Pioglitazone solution, Pioglitazone dispersion, Rosiglitazone solution, Pioglitazone loaded untargeted & transferrin conjugated targeted nanoparticles, and Rosiglitazone loaded untargeted & transferrin conjugated targeted nanoparticles were labeled with ^{99m}Tc by direct labeling method as reported earlier, with slight modifications (Richardson et al., 1977, Liu et al., 1997, Reddy et al., 2005, Meléndez-Alafort et al., 2006). *In vivo* bio-distribution study by gamma scintigraphy was performed in swiss albino mice received from and at, Department of Research, Jawahar Lal Nehru Cancer Hospital & Research Centre, Bhopal, India. Stannous chloride ($SnCl_2$) was purchased from Sigma Aldrich Laborchemikalien GmBH, Germany. Technetium-^{99m} (as pertechnetate) ($^{99m}TcO_4^-$) was obtained from Nuclear Medicine Department, Jawahar Lal Nehru Cancer Hospital & Research Centre, Bhopal.

Briefly, 0.1 mL of ^{99m}Tc (1mCi/mL)(obtained by solvent extraction method from molybdenum) in saline was mixed with 0.1 ml of stannous chloride solution (2 mg/ml) in 10% acetic acid (1 mg/mL) and this solution was kept at room temperature (RT) after adjustment of the pH to 7.0 using 0.5 M sodium bicarbonate solution. To this solution, 1 mL of Pioglitazone/Rosiglitazone solution (1 mg/mL) was added and incubated for 30 minutes at RT to obtain radio-labeled drug solution. All other formulations were also radiolabeled in the same way and were stored in sterile evacuated sealed vials for subsequent studies.

8.2 RADIOLABELING EFFICIENCY & RADIOCHEMICAL PURITY

Radiolabeling efficiency and radiochemical purity was determined by ascending instant thin layer chromatography (ITLC) (Saha, 2004; Reddy et al., 2005; Panwar et al., 2007) using silica gel coated fiber sheets (Gelman Science Inc., Ann Arbor, MI, USA). ITLC was performed using 100% acetone as mobile phase. A measured amount of 2-3 µL of the radiolabeled complex was applied at a point 1 cm from one end of an ITLC-SG strip. The strip was developed in acetone and the solvent front was allowed to reach 8 cm from the origin. The strip was cut into two equal halves and the radioactivity in each segment was determined in a well type gamma ray counter (Gamma ray scintillation counter, Capintec, CRC®-127R Dose Calibrator, USA. Free $^{99m}TcO_4^-$ was found to have R_f 0.9-1.0 whereas the complexed formulations and radiocolloids, if formed, were retained at the point of application. Furthermore, radiochemical purity and labeled efficiency was corrected by subtracting the migrated activity of unwanted radio colloids in pyridine : acetic acid : water (3:5:1.5). The radio colloids remained at the bottom of the strip, while both the free pertechnetate ($^{99m}TcO_4^-$) and the labeled complex migrated with the solvent front. Percent labeling efficiency was calculated from the following formula:

$$\text{Labeling efficiency (\%)} = \frac{B \times 100}{T + B}$$

where, T is the radio counts at top and B is the radio counts at bottom of the strip. The process of radiolabeling was optimized for the amount of stannous chloride (in the range of 50 - 250 µg), pH (5.0 - 8.0) and incubation time (0-60 min).

8.3 OPTIMIZATION OF RADIOLABELING PROCESS

Various factors could influence the radiolabeling of formulations. Some of the parameters such as the amount of stannous chloride, pH of incubation medium and incubation time were optimized and characterized for the radio-labeling efficiency of the nanocarriers with ^{99m}Tc.

Optimization of amount of stannous chloride:

This study was performed to determine the optimum amount of stannous chloride required for the maximum radiolabeling efficiency. ^{99m}Tc (0.1 ml, approx. 1 mCi/ml) was mixed with 100 µl of stannous chloride solution of different concentrations (25-200 µg/0.1 ml) and all formulations were incubated with the above solutions for 30 minutes. Radiolabeling efficiency of the drugs and different formulations was determined by ITLC method as described in **Section 8.2.** The results of the radiolabeling efficiency are recorded in **Table 8.1 - 8.2** and graph-ically presented in **Fig. 8.1 - 8.2.**

Optimization of pH of incubation medium:

To study the effect of pH on the radiolabeling efficiency, the radiolabeled complexes were incubated at different pH keeping the other variables constant. Radiolabeling efficiency was determined and the results are recorded in **Table 8.3 - 8.4** and graphically shown in **Fig. 8.3 - 8.4.**

Optimization of incubation time:

The effect of incubation time on the radiolabeling efficiency was studied by incubating drugs and formulations with ^{99m}Tc for various time intervals keeping the other variables constant. Radiolabeling efficiency of the drugs and different formulations was determined and the results are recorded in **Table 8.5 - 8.6** and graphically shown in **Fig. 8.5 - 8.6.**

8.4 BIODISTRIBUTION STUDY OF ^{99m}Tc LABELED PIOGLITAZONE / ROSIGLITAZONE FORMULATIONS

Biodistribution study was performed in normal, healthy, Swiss Albino mice of either sex weighing about 20–25 g. All animal studies were carried out in accordance with the guidelines prescribed by CPCSEA (Committee for the Purpose of Control and Supervision of Experiments on Animals, Ministry of Social Justice and Empowerment, Government of India) and all the animal study protocols were approved by Institutional Animal Ethics Committee of Jawahar Lal Nehru Cancer Hospital & Research Centre, Bhopal, India (Protocol No. 2004/EC/2010 - 18-11-2010). The animal experimentation was carried out in the Department of Nuclear Medicine, Jawahar Lal Nehru Cancer Hospital and Research Centre, Bhopal, India.

The organ distribution of PIO-S, PIO-D, ROS-S, PIO-NP, Tf-PIO-NP, ROS-NP and Tf-ROS-NP labeled with ^{99m}Tc was studied following intravenous/ intranasal/oral administration.

All the animals (swiss albino mice) received a standard commercial pellet diet and water *ad libitum*, and were fasted overnight prior to experiment. The animals were divided into ten groups of 3 animals each. Respective groups were administered with intravenous, oral or intranasal dose of 15 mg/kg body weight of pioglitazone and 1.5 mg/kg body weight of rosiglitazone in the form of radio labeled formulations. The injection volume was adjusted to 0.1 ml/100 g of mouse weight and nasal solution volume was fixed to be 0.1 ml in each nostrils. PIO-NP and Tf-PIO-NP in PBS were randomly injected to animals of first and second group respectively in the tail vein. The radiolabeled ROS-S, ROS-NP and Tf-ROS-NP formulations were randomly injected in the tail vein of animals of

third, fourth and fifth groups. Animals of sixth and seventh group were orally administered with PIO-D and ROS-S in PBS. Eighth and ninth group animals were intranasally administered with PIO-S and ROS-S (nasal solution in PBS). The animals of tenth group were kept as control.

After 0.5, 1, 2 and 6 hrs of administration, the mice were sacrificed by cervical dislocation and their organs such as brain, liver, spleen, lungs, kidneys and heart were excised, washed quickly with cold water to remove surface blood and dried using tissue paper. The organs were taken in pre-weighed tubes, which were weighed again to calculate the weight of organ/tissue and radioactivity corresponding to them was measured using well-type γ-scintillation counter. Blood samples (1 mL) were also obtained in duplicate by cardiac puncture in pre-weighed heparinized tubes. The biodistribution of ^{99m}Tc-labelled Pioglitazone (oral/nasal), Pioglitazone loaded untargeted & transferrin conjugated targeted nanoparticles (i.v.), Rosiglitazone solution (i.v./oral/nasal), Rosiglitazone loaded untargeted & transferrin conjugated targeted nanoparticulate formulations (i.v.) in each organ was calculated as a percentage of the injected dose per gram of the tissue **(%ID/g).** The observations are recorded in **Table 8.7 - 8.15** and represented graphically in **Fig. 8.7 - 8.17.** The radioactivity remaining in the tail at the end was also measured and taken into consideration in the calculation of total radioactivity dose administered to the mice.

For gamma imaging studies, the animals were fixed on wooden boards by sticking with adhesive tape without applying pressure so that the animals did not feel uneasiness and their normal metabolic activity was not disturbed. Just before sacrificing the animals for organ distribution studies at 0.5, 1, 2 and 6 hrs time intervals, bio-imaging was performed on animals fixed on wooden board using E-Cam Single Head Gamma Camera (Siemen's, Germany) **(Fig. 8.18 - 8.21).**

Table 8.1: Effect of amount of Stannous Chloride on radiolabeling efficiency of PIO and its nanoparticulate formulations with ^{99m}Tc

Amount of $SnCl_2$ (µg)	% Radiolabeling		
	PIO-S	PIO-NP	Tf-PIO-NP
50	82.53 ± 1.34	69.36 ± 2.74	59.51 ± 1.91
100	90.34 ± 1.11	86.84 ± 1.09	85.53 ± 2.35
200	96.42 ± 0.96	96.15 ± 1.46	97.86 ± 1.49
250	96.02 ± 0.84	95.59 ± 0.94	93.58 ± 1.21

The results are expressed as mean ± S.D. (n=3)

Table 8.2: Effect of amount of Stannous Chloride on radiolabeling efficiency of ROS and its nanoparticulate formulations with ^{99m}Tc

Amount of $SnCl_2$ (µg)	% Radiolabeling		
	ROS-S	ROS-NP	Tf-ROS-NP
50	76.43 ± 1.21	64.85 ± 0.88	63.78 ± 1.24
100	91.96 ± 1.89	83.45 ± 1.39	87.76 ± 1.49
200	97.05 ± 0.94	98.11 ± 1.42	98.17 ± 1.34
250	95.32 ± 1.79	94.44 ± 1.19	95.85 ± 0.76

The results are expressed as mean ± S.D. (n=3)

Table 8.3: Effect of pH on radiolabeling efficiency of PIO and its nanoparticulate formulations with ^{99m}Tc

pH	% Radiolabeling		
	PIO-S	PIO-NP	Tf-PIO-NP
5.0	79.51 ± 1.12	82.49 ± 1.47	84.25 ± 1.29
5.5	83.56 ± 1.58	86.23 ± 0.98	87.49 ± 1.68
6.0	88.39 ± 1.21	91.72 ± 1.54	91.31 ± 1.79
6.5	92.78 ± 1.61	95.58 ± 1.77	95.78 ± 1.01
7.0	98.83 ± 1.39	98.14 ± 1.10	97.83 ± 0.90
8.0	95.11 ± 1.09	94.23 ± 1.22	94.66 ± 1.19

The results are expressed as mean ± S.D. (n=3)

Table 8.4: Effect of pH on radiolabeling efficiency of ROS and its nanoparticulate formulations with ^{99m}Tc

pH	% Radiolabeling		
	ROS-S	ROS-NP	Tf-ROS-NP
5.0	78.10 ± 1.09	83.01 ± 1.45	84.83 ± 1.88
5.5	84.36 ± 1.26	87.37 ± 1.69	86.59 ± 1.52
6.0	89.29 ± 1.89	92.85 ± 1.54	91.36 ± 1.48
6.5	93.08 ± 1.37	94.54 ± 1.32	94.85 ± 1.28
7.0	98.22 ± 0.88	98.06 ± 0.95	98.13 ± 0.78
8.0	94.63 ± 1.56	95.56 ± 0.88	95.83 ± 1.38

The results are expressed as mean ± S.D. (n=3)

Table 8.5: Effect of incubation time on radiolabeling efficiency of PIO and its nanoparticulate formulations with ^{99m}Tc

Incubation Time (Min)	% Radiolabeling		
	PIO-S	PIO-NP	Tf-PIO-NP
0	79.51 ± 1.91	76.36 ± 0.94	80.51 ± 1.20
5	95.34 ± 1.25	97.84 ± 1.58	97.16 ± 1.08
15	98.12 ± 1.08	98.15 ± 0.88	98.22 ± 1.16
30	98.02 ± 1.34	98.34 ± 0.78	98.58 ± 0.80
60	97.35 ± 0.84	96.92 ± 1.40	96.48 ± 1.08

The results are expressed as mean ± S.D. (n=3)

Table 8.6: Effect of incubation time on radiolabeling efficiency of ROS and its nanoparticulate formulations with ^{99m}Tc

Incubation Time (Min)	% Radiolabeling		
	ROS-S	ROS-NP	Tf-ROS-NP
0	78.52 ± 1.84	77.85 ± 1.98	79.78 ± 1.72
5	96.96 ± 1.23	95.45 ± 1.34	94.76 ± 1.12
15	97.05 ± 1.32	97.11 ± 1.18	96.37 ± 1.02
30	98.32 ± 0.96	98.24 ± 0.84	98.85 ± 0.78
60	96.90 ± 1.67	97.70 ± 1.46	96.13 ± 1.10

The results are expressed as mean ± S.D. (n=3)

Table 8.7: Biodistribution of PIO-D (oral)

Organ	% ID/g recovered at different time (hrs)			
	0.5	1	2	
Blood	10.94±0.18	14.18±0.22	21.88±0.12	12.54±0.24
Liver	4.92±0.26	8.48±0.14	14.21±0.05	19.36±0.28
Spleen	1.44±0.18	2.12±0.16	5.56±0.34	3.14±0.12
Kidney	1.26±0.28	2.38±0.42	2.12±0.46	2.24±0.32
Heart	1.04±0.16	4.98±0.39	5.26±0.34	3.86±0.28
Lung	1.88±0.28	2.19±0.40	3.14±0.62	1.48±0.68
Brain	0.02±0.01	0.06±0.02	0.04±0.01	0.03±0.01

The results are expressed as mean ± S.D. (n=3)

Table 8.8: Biodistribution of PIO-S (nasal)

Organ	% ID/g recovered at different time (hrs)			
	0.5	1	2	6
Blood	9.82±0.20	18.86±0.18	16.96±0.24	11.72±0.16
Liver	3.89±0.20	6.52±0.16	13.46±0.18	17.84±0.44
Spleen	1.29±0.16	1.92±0.34	4.58±0.28	4.88±0.19
Kidney	0.38±0.08	1.46±0.38	4.22±0.62	3.38±0.43
Heart	0.24±0.06	1.92±0.46	4.18±0.68	4.40±0.10
Lung	1.94±0.12	2.48±0.38	3.44±0.84	2.58±0.24
Brain	0.05±0.01	0.11±0.02	0.24±0.04	0.22±0.02

The results are expressed as mean ± S.D. (n=3)

Table 8.9: Biodistribution of PIO-NP (i.v.)

Organ	% ID/g recovered at different time (hrs)			
	0.5	1	2	6
Blood	30.23±1.32	24.47±0.73	17.03±0.59	9.31±0.23
Liver	4.34±0.24	7.16±0.18	12.48±0.28	10.58±0.42
Spleen	1.23±0.10	2.24±0.38	6.88±0.32	5.16±0.20
Kidney	1.58±0.18	3.52±0.36	3.88±0.54	3.12±0.32
Heart	1.38±0.16	7.78±0.42	6.26±0.24	4.52±0.24
Lung	0.92±0.10	1.28±0.27	2.50±0.34	3.10±0.14
Brain	0.025±0.01	0.65±0.02	0.84±0.02	0.72±0.01

The results are expressed as mean ± S.D. (n=3)

Table 8.10: Biodistribution of Tf-PIO-NP (i.v.)

Organ	% ID/g recovered at different time (hrs)			
	0.5	1	2	6
Blood	29.41±1.18	21.32±0.69	14.46±0.64	8.07±0.37
Liver	5.28±0.14	9.22±0.20	14.10±0.12	8.44±0.30
Spleen	1.30±0.14	3.46±0.30	6.72±0.18	7.10±0.22
Kidney	1.49±0.12	2.60±0.23	3.68±0.50	2.74±0.34
Heart	1.26±0.10	6.48±0.22	5.10±0.14	3.25±0.20
Lung	0.22±0.08	0.36±0.06	0.40±0.08	1.52±0.10
Brain	0.54±0.08	1.14±0.12	1.92±0.22	2.23±0.31

The results are expressed as mean ± S.D. (n=3)

Table 8.11: Biodistribution of ROS-S (oral)

Organ	% ID/g recovered at different time (hrs)			
	0.5	1	2	6
Blood	11.42±0.14	15.28±0.12	24.08±0.16	14.86±0.18
Liver	3.88±0.48	7.56±0.18	16.32±0.18	18.46±0.25
Spleen	1.80±0.12	2.34±0.18	5.08±0.44	4.20±0.12
Kidney	1.36±0.56	2.68±0.34	2.34±0.26	2.06±0.44
Heart	1.20±0.12	4.50±0.28	4.96±0.42	4.16±0.28
Lung	1.62±0.22	2.38±0.64	2.98±0.68	1.68±0.48
Brain	0.03±0.01	0.05±0.02	0.06±0.01	0.04±0.02

The results are expressed as mean ± S.D. (n=3)

Table 8.12: Biodistribution of ROS-S (nasal)

Organ	% ID/g recovered at different time (hrs)			
	0.5	1	2	6
Blood	8.96±0.32	20.34±0.20	14.92±0.12	10.66±0.80
Liver	3.65±0.32	7.45±0.18	16.22±0.12	17.29±0.72
Spleen	1.08±0.20	1.88±0.40	3.98±0.56	4.56±0.60
Kidney	0.42±0.06	1.38±0.42	4.12±0.48	3.82±0.18
Heart	0.32±0.08	1.68±0.50	4.90±0.22	3.98±0.14
Lung	2.12±0.18	2.78±0.42	3.58±0.78	3.04±0.10
Brain	0.04±0.01	0.14±0.02	0.21±0.04	0.19±0.02

The results are expressed as mean ± S.D. (n=3)

Table 8.13: Biodistribution of ROS-S (i.v.)

Organ	% ID/g recovered at different time (hrs)			
	0.5	1	2	6
Blood	30.12±1.27	23.47±0.84	17.42±0.51	8.03±0.37
Liver	6.29±0.31	10.36±0.43	13.82±0.65	9.04±0.41
Spleen	1.26±0.05	3.72±0.14	4.91±0.28	1.73±0.06
Kidney	4.30±0.21	8.40±0.38	9.26±0.41	4.35±0.22
Heart	3.32±0.16	4.09±0.17	3.23±0.15	2.52±0.12
Lung	0.83±0.40	2.38±0.12	2.33±0.13	1.5±0.06
Brain	0.05±0.02	0.07±0.03	0.08±0.04	0.06±0.02

The results are expressed as mean ± S.D. (n=3)

Table 8.14: Biodistribution of ROS-NP (i.v.)

Organ	% ID/g recovered at different time (hrs)			
	0.5	1	2	6
Blood	31.40±1.18	26.22±0.88	19.38±0.48	8.90±0.42
Liver	3.86±0.20	6.20±0.28	11.54±0.18	9.88±0.46
Spleen	1.12±0.10	2.08±0.16	5.96±0.14	5.40±0.11
Kidney	1.32±0.08	3.32±0.15	3.96±0.12	2.94±0.10
Heart	1.08±0.06	8.06±0.22	7.16±0.16	5.02±0.14
Lung	0.84±0.06	1.34±0.08	2.72±0.12	2.98±0.10
Brain	0.034±0.01	0.71±0.02	0.90±0.02	0.78±0.01

The results are expressed as mean ± S.D. (n=3)

Table 8.15: Biodistribution of Tf-ROS-NP (i.v.)

Organ	% ID/g recovered at different time (hrs)			
	0.5	1	2	6
Blood	30.26±1.20	22.28±0.24	15.68±0.10	9.18±0.28
Liver	5.06±0.10	10.34±0.12	15.10±0.16	9.34±0.26
Spleen	1.48±0.18	3.78±0.32	6.08±0.12	6.88±0.20
Kidney	1.54±0.14	2.46±0.18	3.84±0.24	2.48±0.18
Heart	1.38±0.08	6.98±0.14	4.88±0.08	3.80±0.17
Lung	0.30±0.05	0.46±0.06	0.50±0.05	1.74±0.10
Brain	0.64±0.04	1.22±0.08	2.10±0.12	2.46±0.16

The results are expressed as mean ± S.D. (n=3)

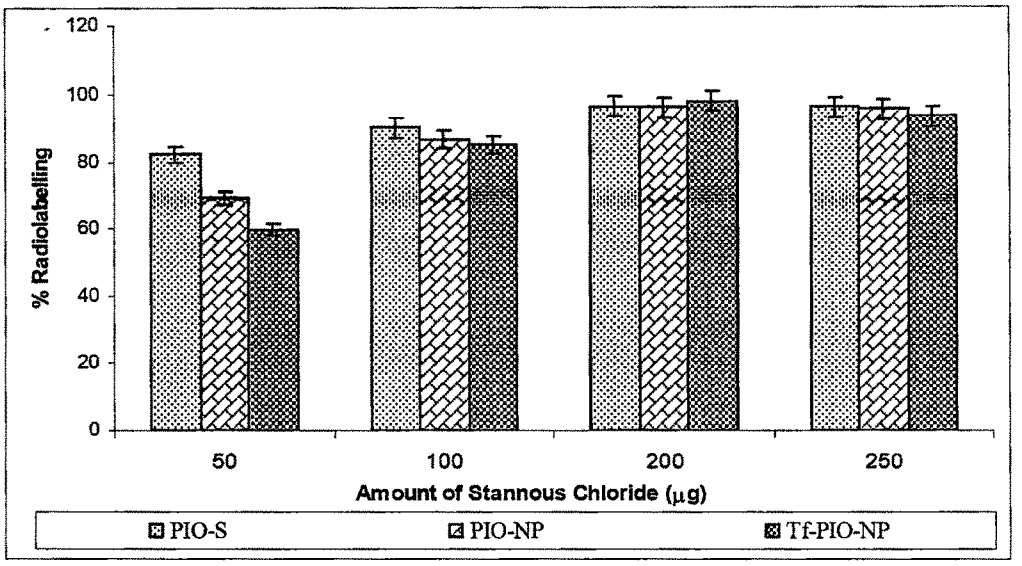

Fig. 8.1: Effect of amount of stannous chloride on labeling efficiency of Pioglitazone and its nanoparticulate formulation with ^{99m}Tc

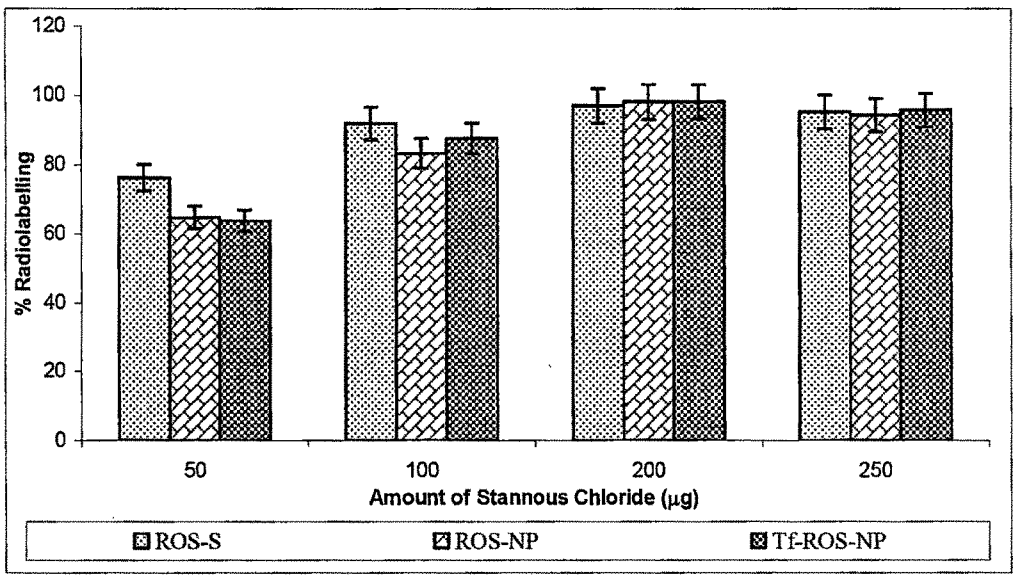

Fig. 8.2: Effect of amount of stannous chloride on labeling efficiency of Rosiglitazone and its nanoparticulate formulation with ^{99m}Tc

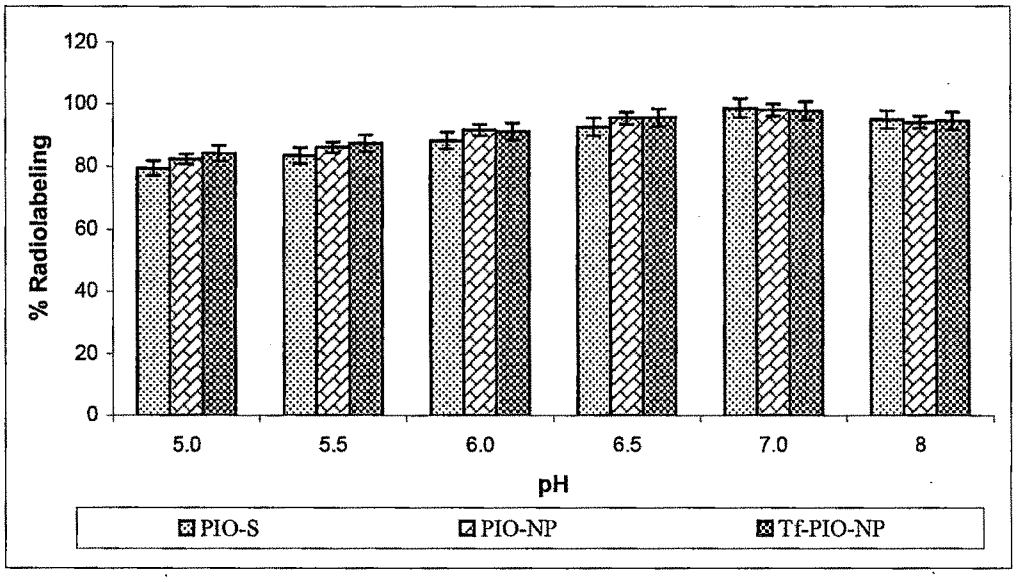

Fig. 8.3: Effect of pH on labeling efficiency of Pioglitazone and its nanoparticulate formulation with ^{99m}Tc

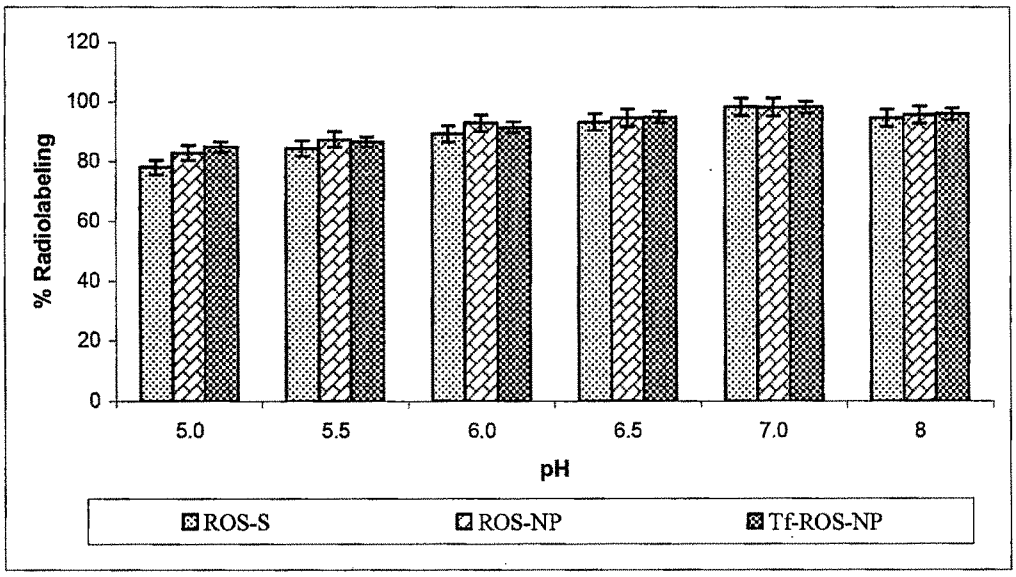

Fig. 8.4: Effect of pH on labeling efficiency of Rosiglitazone and its nanoparticulate formulation with ^{99m}Tc

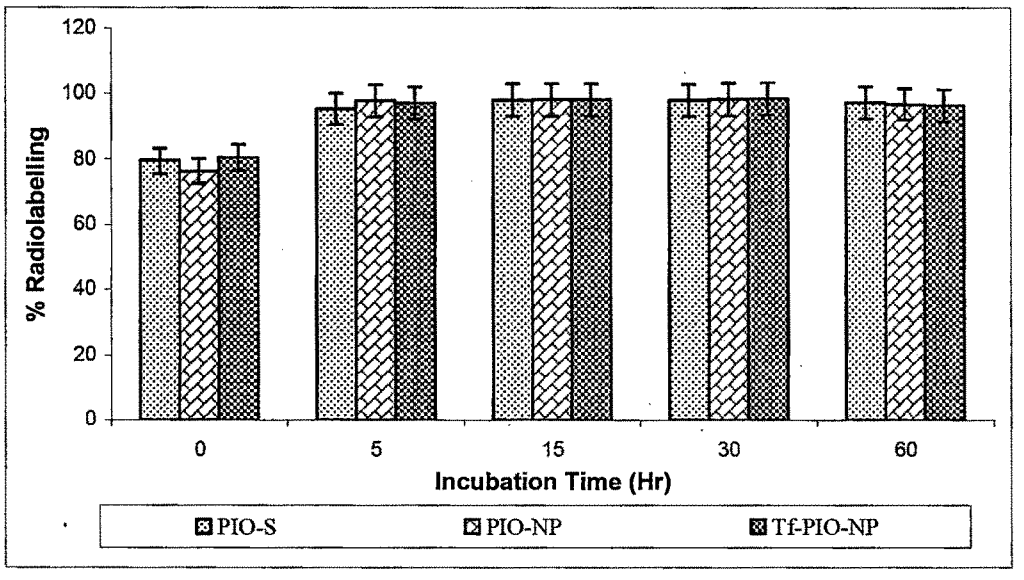

Fig. 8.5: Effect of incubation time on labeling efficiency of Pioglitazone and its nanoparticulate formulation with ^{99m}Tc

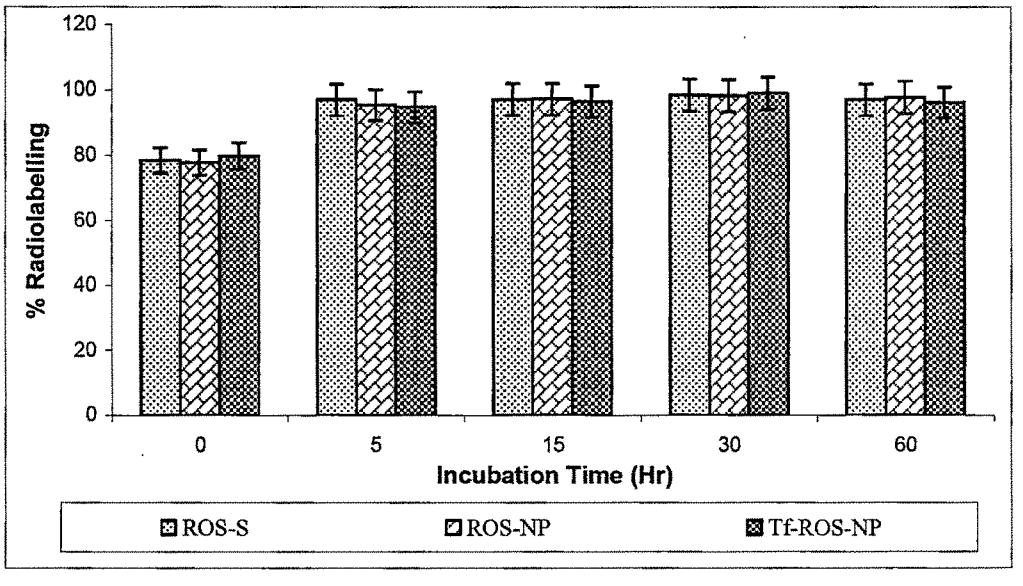

Fig. 8.6: Effect of incubation time on labeling efficiency of Rosiglitazone and its nanoparticulate formulation with ^{99m}Tc

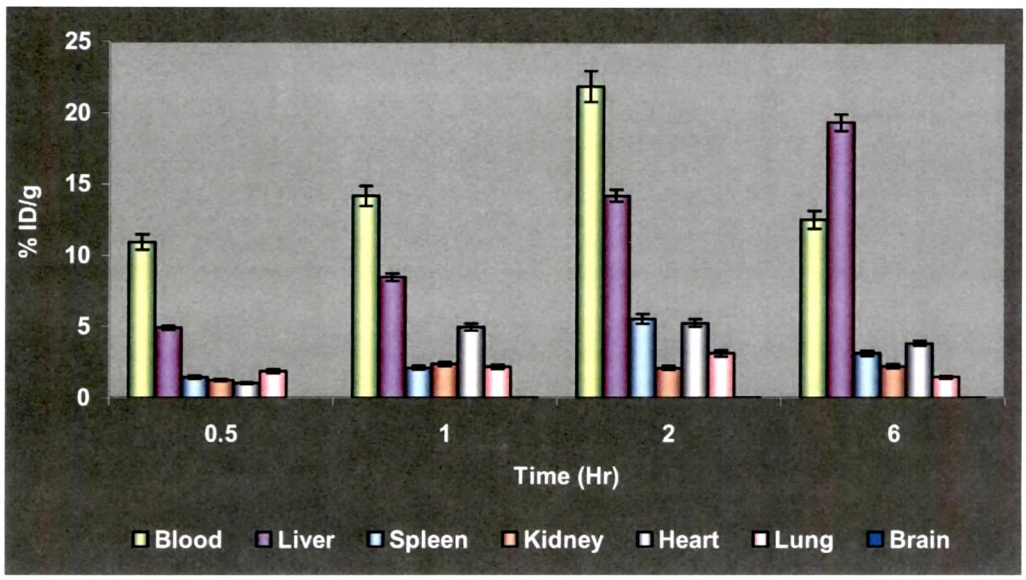

Fig. 8.7: Biodistribution of PIO-D (oral)

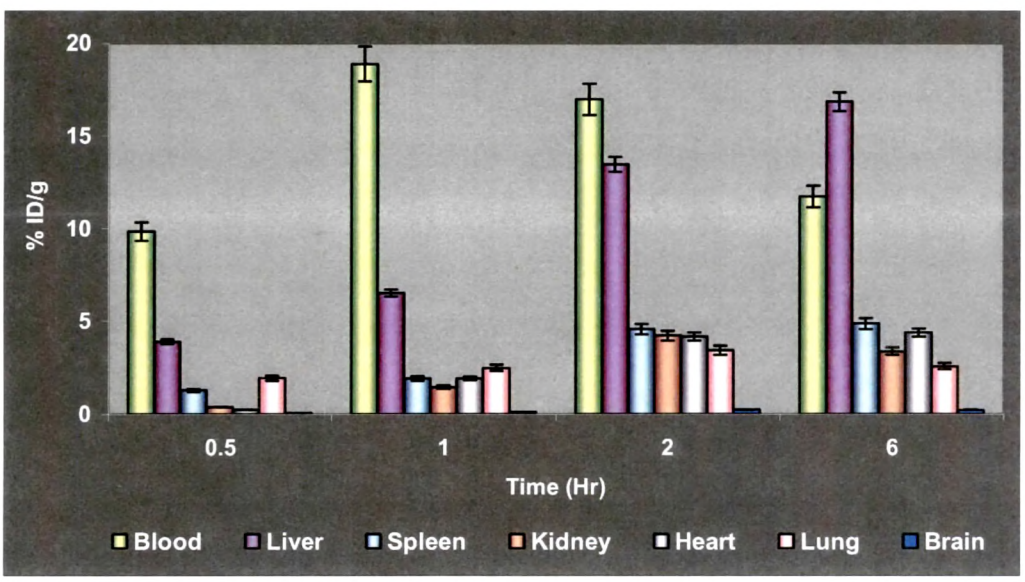

Fig. 8.8: Biodistribution of PIO-S (nasal)

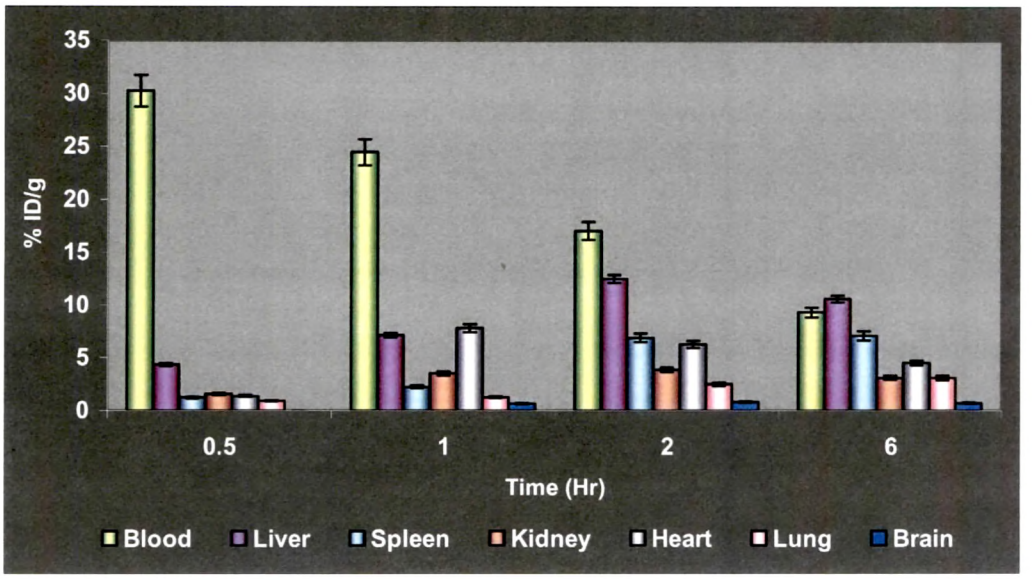

Fig.8.9: Biodistribution of PIO-NP (i.v.)

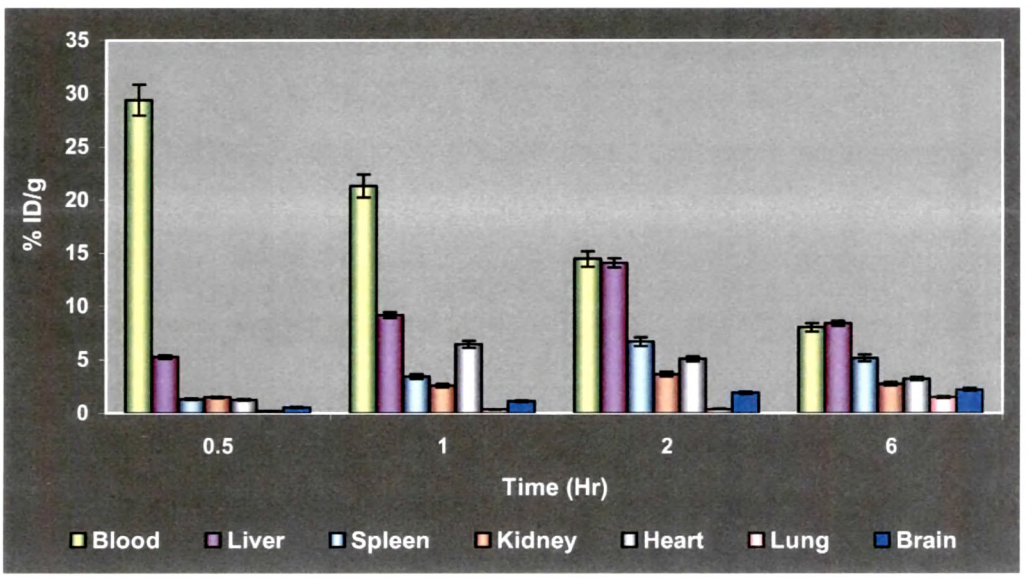

Fig. 8.10: Biodistribution of Tf-PIO-NP (i.v.)

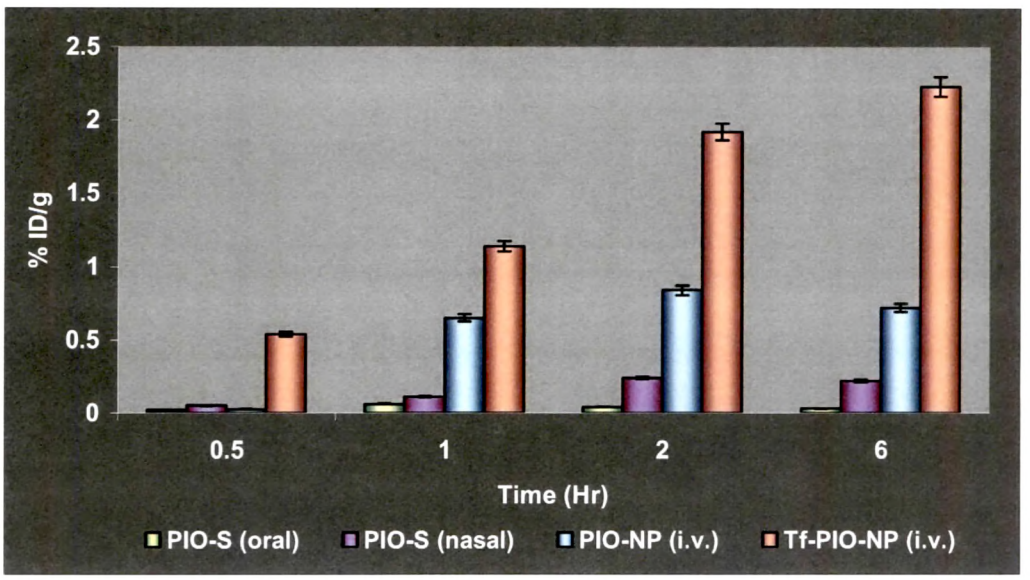

Fig. 8.11: Biodistribution of different Pioglitazone formulations in Brain

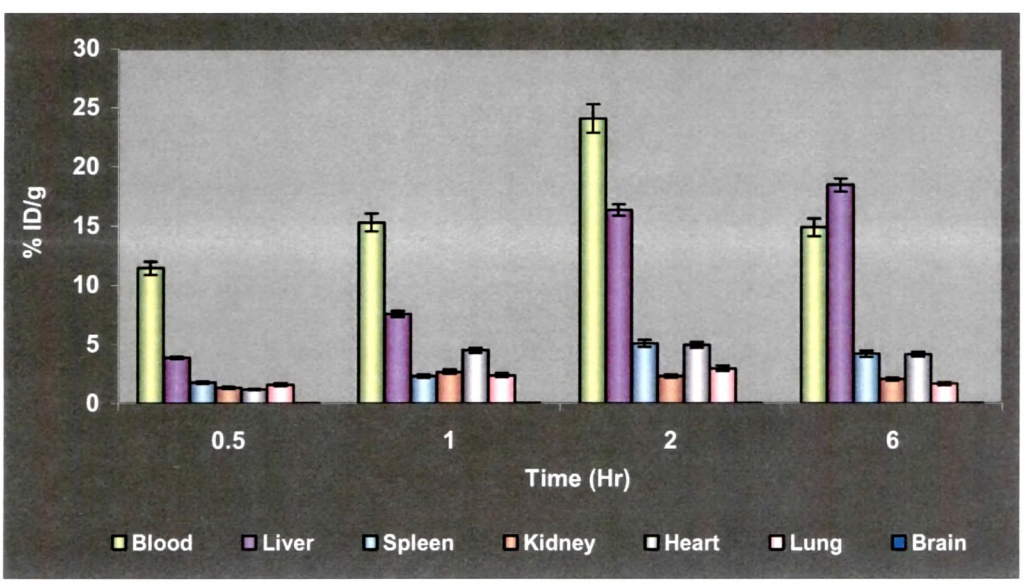

Fig. 8.12: Biodistribution of ROS-S (oral)

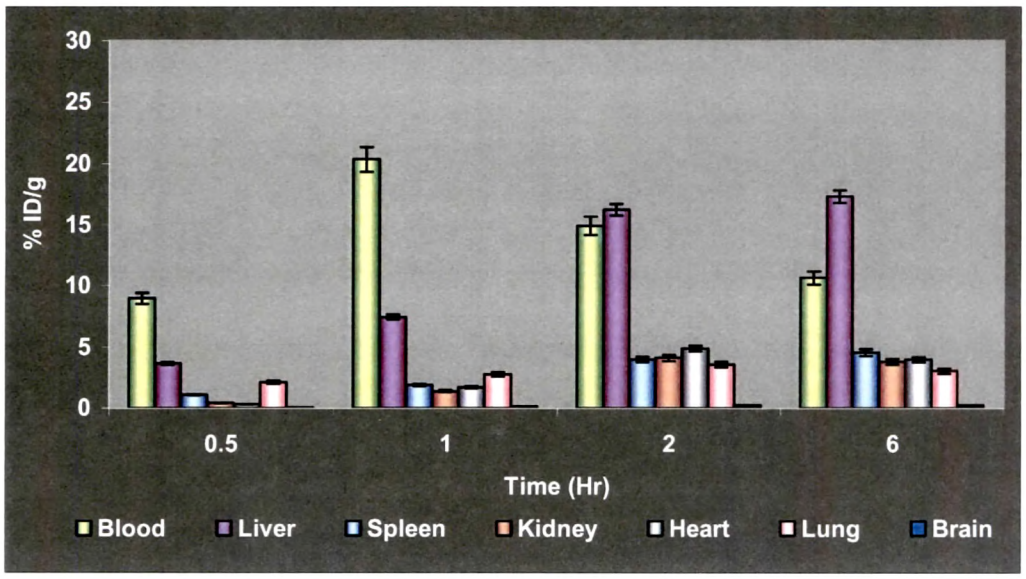

Fig. 8.13: Biodistribution of ROS-S (nasal)

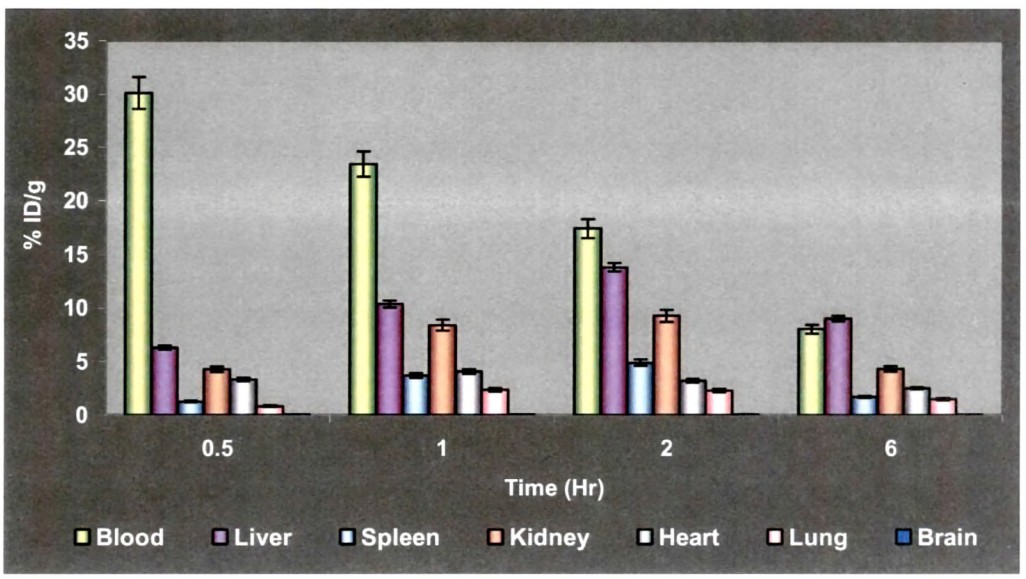

Fig. 8.14: Biodistribution of ROS-S (i.v.)

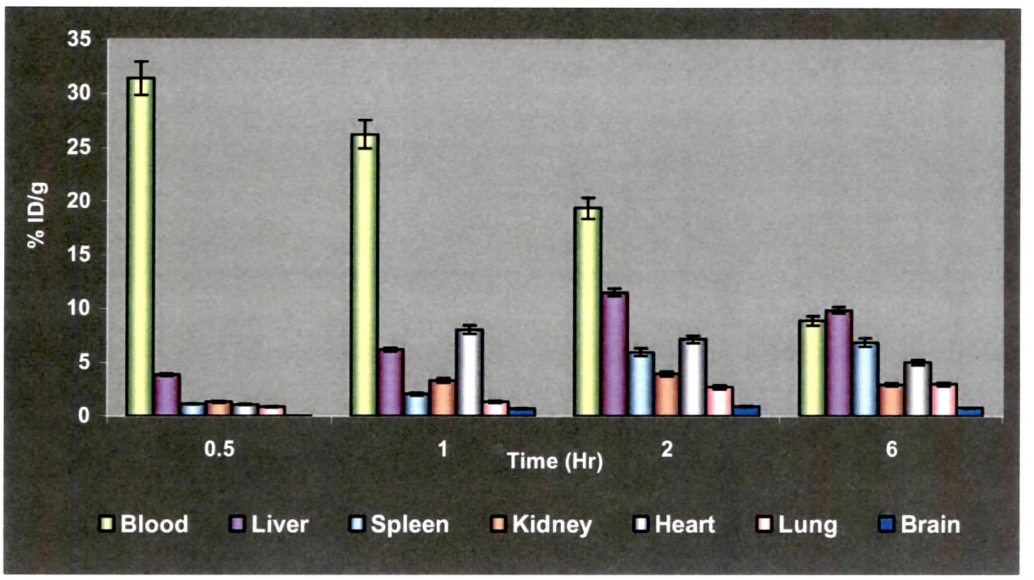

Fig. 8.15: Biodistribution of ROS-NP (i.v.)

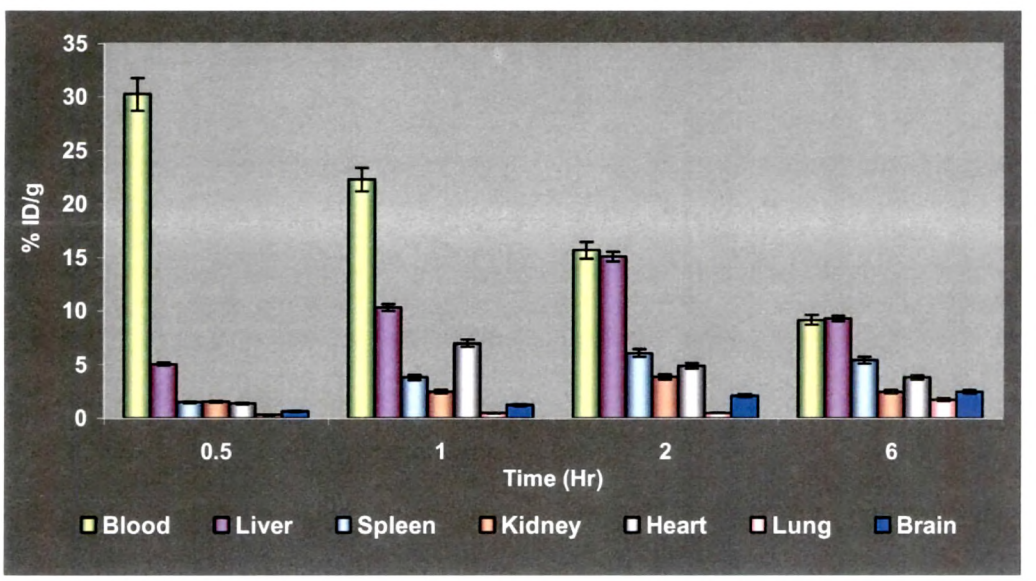

Fig. 8.16: Biodistribution of Tf-ROS-NP (i.v.)

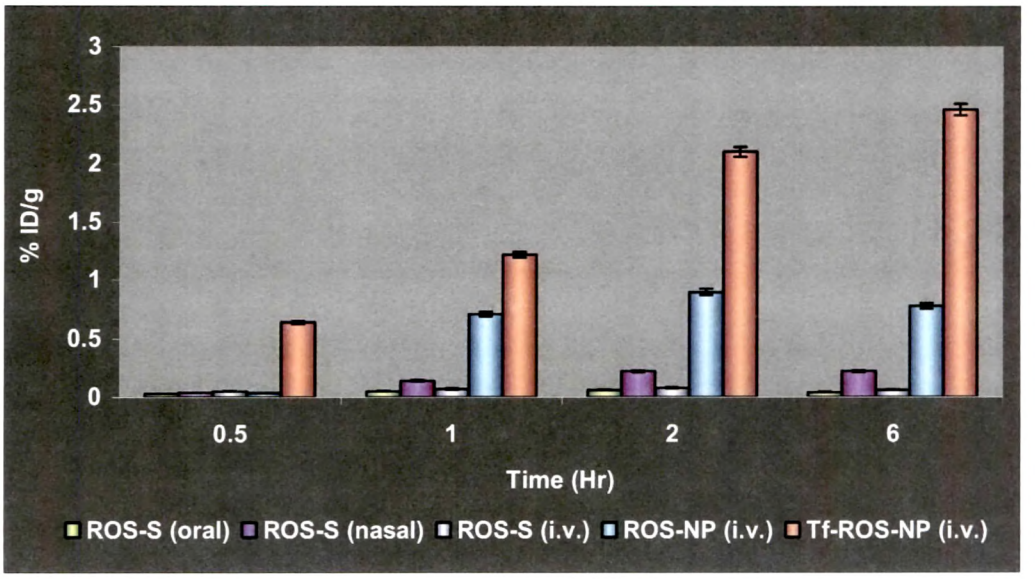

Fig. 8.17: Biodistribution of different Rossiglitazone formulations in Brain

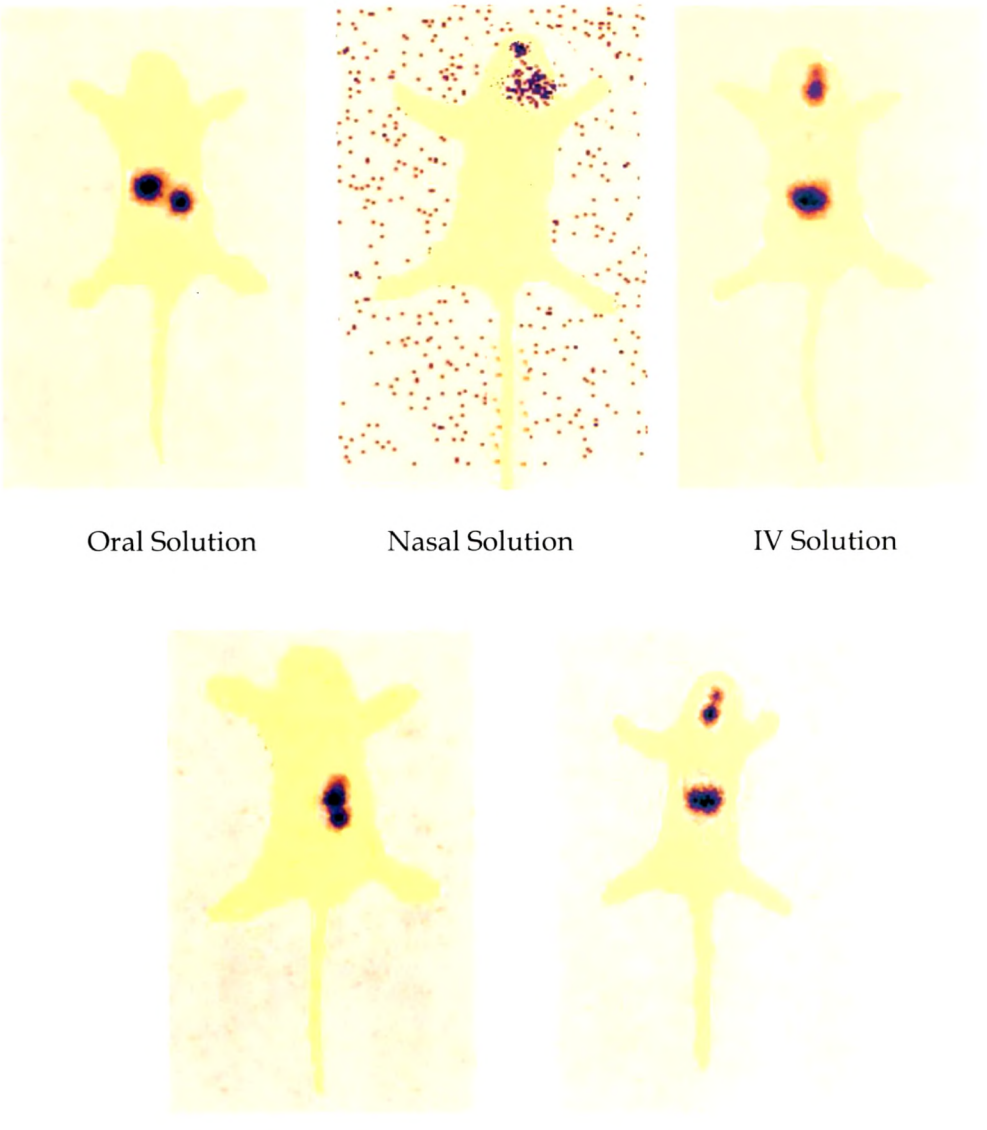

Fig. 8.18: Gamma Scintigraphs of swiss albino mice after administration of radiolabeled formulations at 30 min.

[Oral Solution : drug solution administered through oral route, Nasal Solution : drug solution administered through nasal route, IV Solution : drug solution administered through intravenous route, IV-NP : drug nanoparticles administered through intravenous route, IV-TF-C-NP : transferrin conjugated drug nanoparticles administered through intravenous route]

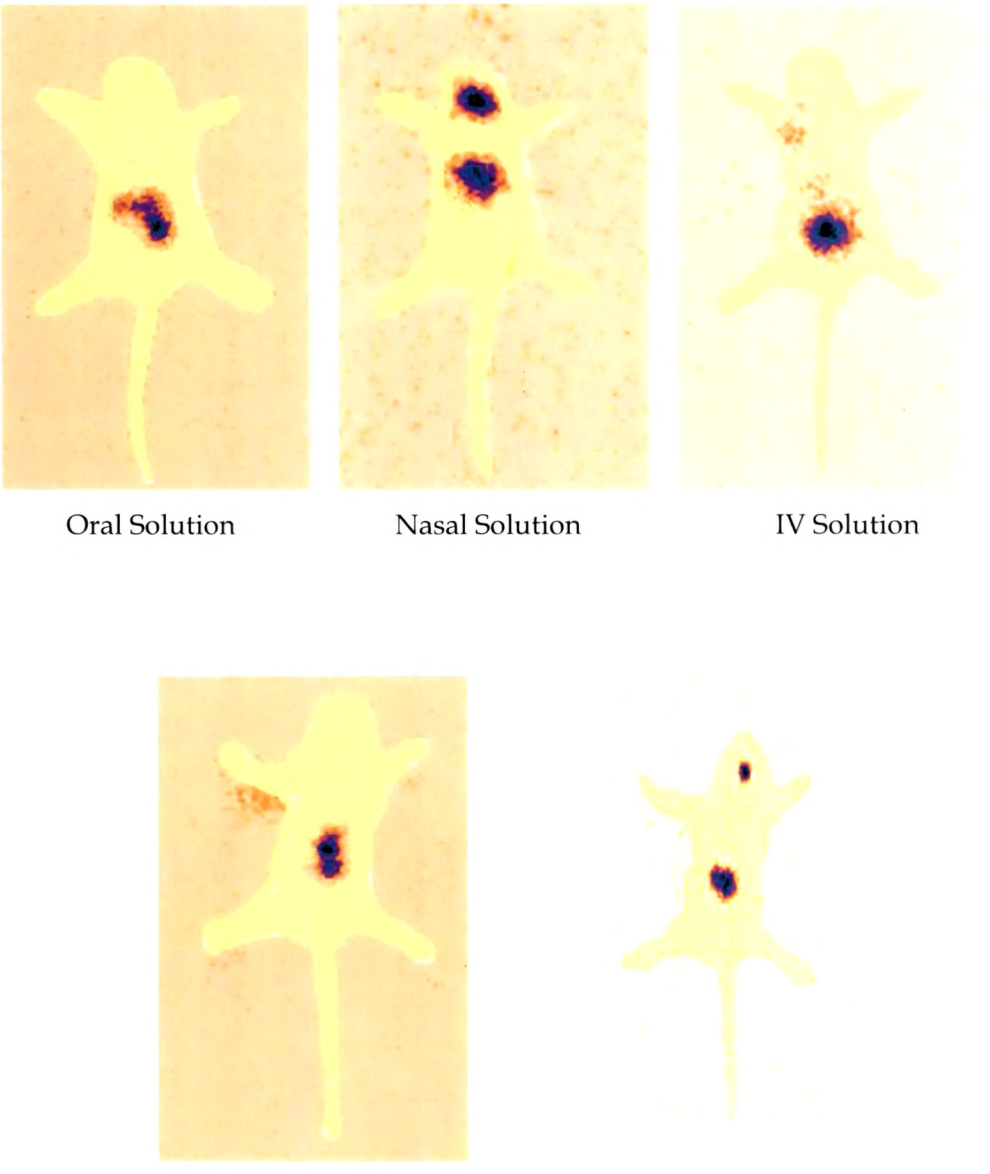

Fig. 8.19: Gamma Scintigraphs of swiss albino mice after administration of radiolabeled formulations at 1 Hr.

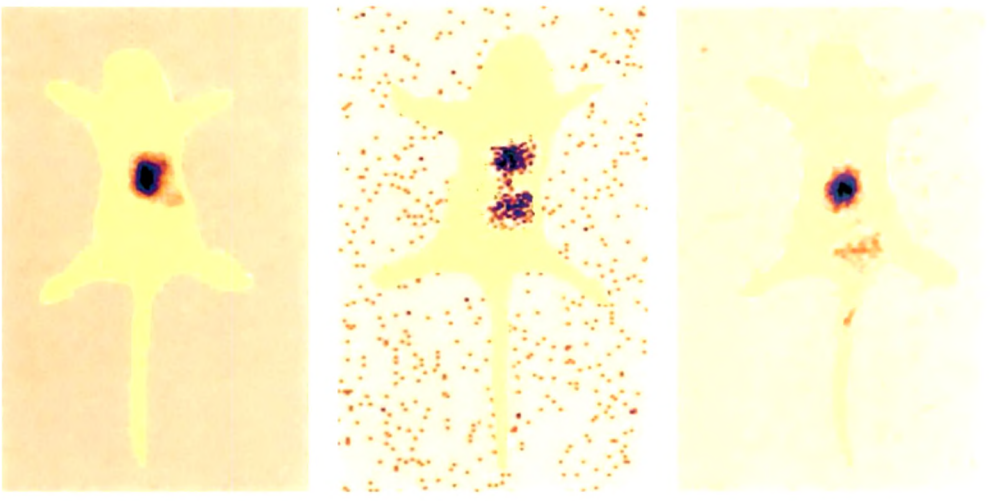

Oral Solution Nasal Solution IV Solution

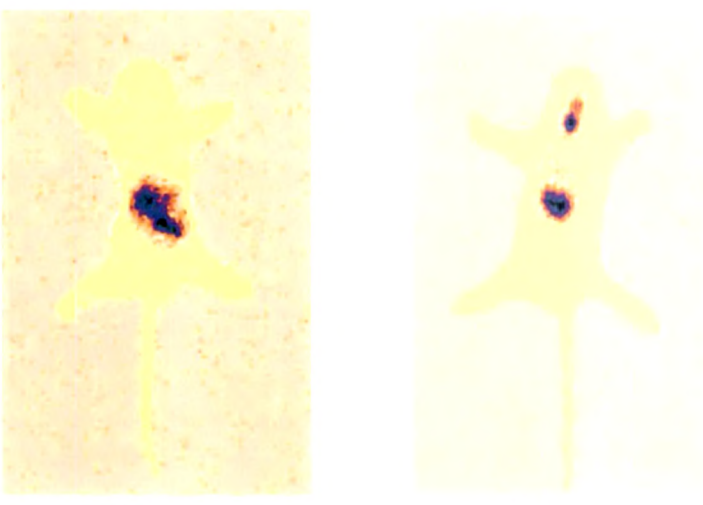

IV-NP IV-TF-C-NP

Fig. 8.20: Gamma Scintigraphs of swiss albino mice after administration of radiolabeled formulations at 2 Hrs.

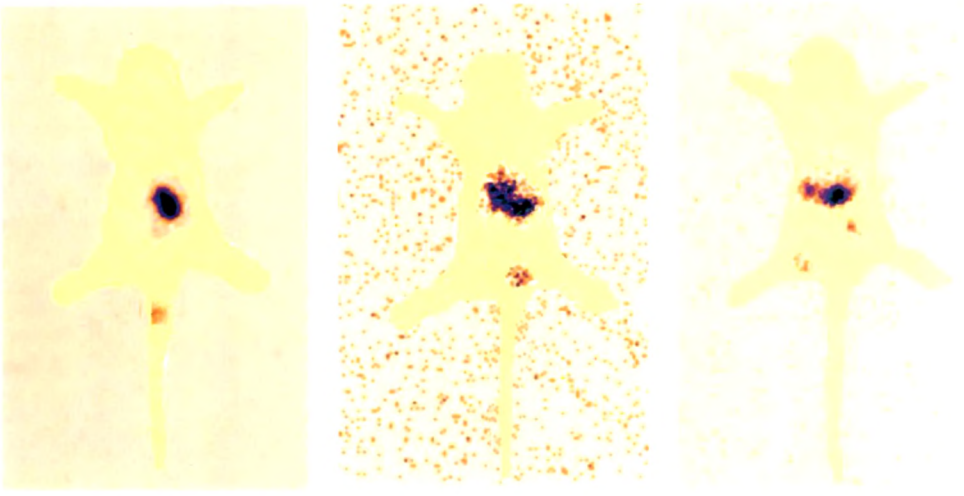

Oral Solution Nasal Solution IV Solution

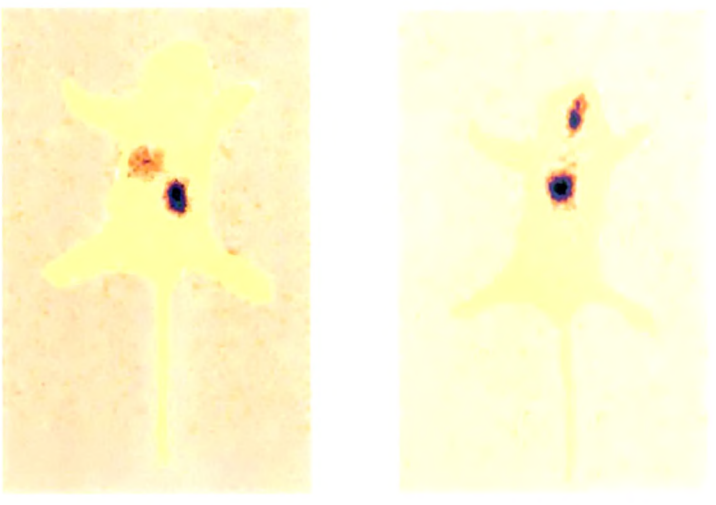

IV-NP IV-TF-C-NP

Fig. 8.21: Gamma Scintigraphs of swiss albino mice after administration of radiolabeled formulations at 6 Hrs.

8.5 RESULTS AND DISCUSSION

Targeted drug delivery systems promise to expand the therapeutic window of drugs by increasing delivery to the target tissue as well as the target to non-target tissue ratio. This in turn led to a reduction in the minimum effective dose of the drug and the accompanying drug toxicity, and an improvement in therapeutic efficacy at equivalent plasma concentrations. Given the often limited number of targeted receptor sites on any given target tissue, targeted delivery is a particularly attractive approach for agents with narrow therapeutic window and/or are active at very low concentrations.

8.5.1 Radiolabeling of Nanoparticulate Formulations

Number of radioactive materials like ^{125}I have been reported for the scintigraphic studies. However, in our study, $^{99m}TcO_4^-$ was used for the radiolabeling of all the nanoparticulate formulations as well as both drugs (Pioglitazone and Rosiglitazone) due to its easy availability, cost effectiveness and low radiation dose. Since half-life of $^{99m}TcO_4^-$ is 6 hrs as compared to 60 days for ^{125}I, it presents lesser radiation burden. ^{99m}Tc was used to directly label preformed conjugates using stannous chloride as a reducing agent. Technetium (^{99m}Tc) used in the study was reduced to its lower valency state (+4) using stannous chloride dihydrate and then pH was adjusted to neutral before mixing it with drug solution and nanoparticles formulations.

Radiolabeling was optimized by taking three factors into consideration i.e. amount of stannous chloride dihydrate, pH of the incubation medium, and incubation time. The amount of reducing agent used for labeling plays a very decisive role in labeling efficiency. A high amount of stannous chloride leads to formation of radiocolloids (reduced/hydrolyzed $^{99m}TcO_4^-$), which is undesirable.

On the other hand, less amount of stannous chloride results in poor labeling (Agashe et al., 2007; Reddy et al., 2004, 2005; Thakkar et al., 2004). It was observed that the addition of 200 μg of stannous chloride resulted in the highest labeling efficiency with minimum amount of R/H or free ^{99m}Tc. At lower concentration of stannous chloride (<200μg/ml) the remaining activity was due to free ^{99m}Tc, whereas at higher concentration (>200μg/ml) radiocolloids were formed (**Table 8.1, 8.2 and Fig. 8.1, 8.2**).

The effect of pH on labeling efficiency is recorded in **Table 8.3, 8.4** and shown in **Fig. 8.3, 8.4**. As the pH was increased from 5 to 7, the radiolabeling also increased from 79.51 to 98.83% for PIO-S, 82.49 to 98.14% for PIO-NP and 84.25 to 97.83% for Tf-PIO-NP nanoparticles. Further increase in the pH resulted in the reduction of radio-labeling efficiency (**Table 8.3** and **Fig. 8.3**). Similar effect of pH was also observed on radiolabeling of Rosiglitazone and its nanoparticlulate formulations (**Table 8.4** and **Fig. 8.4**). The incubation time required for maximum radiolabeling was found to be 30 min for all the formulations (**Table 8.5** and **8.6**). Further increase in incubation time did not show any significant increase in the radiolabeling efficiency (**Fig. 8.5** and **8.6**).

8.5.2 Biodistribution Study of ^{99m}Tc Labeled Formulations

In order to evaluate the potential of nanoparticle uptake by various tissues, the biodistribution of radiolabeled pioglitazone, pioglitazone loaded nanoparticles, rosiglitazone and rosiglitazone loaded nanoparticles was studied in mouse model (swiss albino) for 6 hr after single i.v./oral/nasal administration. The radioactivity observed is reported as percent injected dose per gram of organ/tissue. The **% ID/g** distribution of free drug and its nanoparticles to tissue in different organs at different time intervals are recorded in **Table 8.7 - 8.10** and

shown graphically in **Fig 8.7 - 8.10** for pioglitazone and in **Table 8.11 - 8.15, Fig 8.12 - 8.16** for rosiglitazone. The comparative brain distribution profile of different formulations of Pioglitazone and Rosiglitazone is depicted in **Fig. 8.11 & Fig. 8.17**, respectively.

Upon oral administration of rosiglitazone, initially the drug level in plasma increased upto 2 hrs after which it decreased. This may be due to its short half-life ($t_{1/2}$) of 3-4 hrs. After i.v. administration of ROS-S, plasma drug level dropped rapidly in the initial phase but was slowly declined in the terminal phase. After administration of ROS-NP and Tf-ROS-NP, the plasma level of radioactivity associated with nanoparticles decreased relatively slowly in the initial phase and remained at higher levels in the terminal phase (**Fig. 8.15 & 8.16**), resulting in longer systemic retention of the drug. The plasma profile study of pioglitazone formulations after systemic administration also gave similar results. However the nanoparticulate systems due to their ability to control the release of drugs maintained the drug concentration in blood for longer period in comparison to free drug. Both types of nanoparticulate formulations i.e. unconjugated and transferrin conjugated lead to enhanced plasma level of the drug in the body, which was an important rationale of the therapy. Similar results have been reported by other researchers also (Gan and Feng, 2010).

Upon oral administration of PIO-D, highest radioactivity was recovered from liver (19.36±0.28 % ID/g) at the end of 6 hrs. Similar results were obtained with ROS-S, where highest radioactivity was recovered from liver (18.46±0.25 %ID/g) after oral administration. Furthermore, insignificant radioactivity was detected in brain in both the cases (0.03±0.01 % ID/g and 0.04±0.02 % ID/g in case of PIO-D and ROS-S, respectively). Here it needs to be mentioned that rosiglitazone is unable to cross BBB when orally administered (Pedersen and

Flynn, 2004; Risner et al., 2006) and pioglitazone has minimal BBB permeability (Maeshiba et al., 1997) and this is confirmed by these results also.

Upon intranasal delivery, highest radioactivity was again recovered from liver and was 17.84±0.44 % and 17.29±0.72 % ID/g in case of PIO-S and ROS-S, respectively, at the end of 6 hrs. Further, some radioactivity was also recovered from brain (0.22±0.02 % ID/g and 0.19±0.02 % ID/g with PIO-S and ROS-S, respectively) at the end of 6 hrs. This indicates the direct transport of the drug to the brain through the olfactory route thus bypassing the blood brain barrier (Illum, 2000). However, this amount of radioactivity and hence the drug delivered to brain may not be considered to be high enough to be able to produce any remarkable therapeutic effect. When ROS-S was intravenously administered, the radioactivity recovered in the liver was 9.04±0.41 % ID/g. The results obtained may be attributed to liver being the major organ of metabolism of the drug(s). Since liver and kidneys are the major organs for distribution of ROS, the maximum drug accumulated in liver within 2 hrs of injection of drug solution which declined slowly. Pioglitazone was not injected in solution form intravenously as it is soluble in DMSO which cannot be administered I.V. due to its toxicity. Therefore, Pioglitazone/Rosiglitazone was encapsulated in PLGA nanoparticles; subsequently transferrin was conjugated for brain targeting and the formulation was injected intravenously.

Transferrin conjugated rosiglitazone nanoparticles (i.v.) showed greatest radioactivity in brain in comparison to ROS-S (oral, intranasal, i.v.) or ROS-NP (i.v.). Although the amount of radioactivity measured in brain tissue included the total level of radioactivity both outside i.e. in capillaries and beyond the BBB, the higher level of radioactivity and hence drug in the brain could be attributed

to the drug being transported across the BBB by Tf-conjugated nanoparticles. Six hrs after injection of ROS-S, very low radioactivity was detected in brain.

The distribution of rosiglitazone when administered as i.v. solution was more in kidney in comparison to unconjugated and Tf conjugated nanoparticles. At 0.5 hrs after intravenous injection, rosiglitazone showed higher accumulation in kidney at 4.30±0.21 %ID/g with respect to 1.32±0.08 %ID/g for ROS-NP and 1.54±0.14 %ID/g for Tf-ROS-NP, indicating fast clearance of drug solution from kidney than the nanoparticulate formulation. Kidney is highly involved in eliminationof ROS, which excretes a variety of waste products produced by metabolism. The CVS side effect associated with rosiglitazone is due to its effect on glomerular filtration. In the present study, high amount of radioactivity was detected in the kidney following administration of ROS-S while administration of Tf-conjugated nanoparticles resulted in a decrease in radioactivity in the kidney which will consequently reduce its CVS side effects.

The radioactivity measured in lungs indicates higher accumulation of unconjugated nanoparticles than free drug's after 6 hrs where as Tf-conjugated nanoparticles showed lung distribution equivalent to that of free drug's. This enhanced deposition of NP's may be due to the size and particulate nature of the nanoparticles while Tf-conjugated nanoparticles got localized to the Tf receptor expressing organs.

Based on the radioactivity measurement in different organs, it could be concluded that organs of reticulo-endothelial system were responsible for a major uptake of the drug when administered as solution. The study also suggested that modulation with Tf did not affect the RES uptake of nanoparticles. As shown previously, large proportion of the nanoparticles was recovered from the liver and spleen (>5% ID/g organ), suggesting that these are

the major clearance organs even for Tf-conjugated nanoparticles. Active uptake mechanisms such as phagocytosis by Kupffer's cells in the liver, or filtration by a meshwork consisting of reticular fibers and accompanying macrophages in the red pulp in spleen can be attributed to these high clearances, as reported previously (Klibanov et al., 1991; Litzinger et al., 1994). The uptake of Tf-conjugated nanoparticles in spleen was further enhanced as compared to unconjugated nanoparticles, presumably because large nanoparticles were efficiently trapped by filtration, as shown previously (Klibanov et al., 1991; Liu et al., 1992; Litzinger et al., 1994). The results also suggested that free drugs had large access to liver, heart and spleen when orally administered whereas after i.v. administration, only liver and kidney were the major sites for drug accumulation (**Table 8.7, 8.11, 8.13**). The radioactivity detected in the heart was significantly decreased in animals administered with unconjugated nanoparticles or Tf-conjugated nanoparticles as compare to when drug solution was administered. This could be related to the encapsulation of drug in the nanoparticles which prevented its localization in the heart. Myocardial tissue is relatively compact, making the nanoparticles less likely to extravasate from small blood vessels, which may explain why nanoparticles are less likely to accumulate in the heart than the free drug.

In the present study, Tf-dependent uptake was observed with Tf-conjugated nanoparticles in the liver, brain and heart suggesting that Tf-conjugated nanoparticles were taken up by Tf receptor-mediated endocytosis. This can be attributed to the differences in the density of Tf-receptors or internalization rate via endocytosis among these organs. On the other hand, in other organs such as lungs, Tf-dependent uptake was barely detectable, inspite

of the high or ubiquitous expression of Tf receptors (Ponka and Lok, 1999; Qian et al., 2002). These results are not in agreement with prior observations.

Biodistribution profile of Pioglitazone loaded nanoparticles was similar to that of Rosiglitazone loaded nanoparticles possibly because targeting of drug delivery systems relies on the carrier system itself and not on the entrapped drug. Nanoparticles showed enhanced circulation time when compared with free drug's. Transferrin conjugated nanoparticles encapsulating Pioglitazone showed greater localized radioactivity in brain as compared to intranasal administered drug solution. However, in case of PIO-NP, slightly increased radioactivity as compared to intranasal formulation was recovered from brain.

Transferrin conjugation of nanoparticles altered the biodistribution of drugs. The distribution of Tf-PIO-NP was found to be 2.23±0.31% in brain after 6 hrs post injection which was almost 10 and 3 times more as compared to PIO-S (nasal) and PIO-NP (i.v.), respectively (**Table 8.8, 8.9** and **Fig. 8.11**). Similar results were also observed with Tf-ROS-NP (**Table 8.10**). Thus ligand coupling to the nano-particulate surface has enhanced their delivery to the brain. Hence, receptor mediated endocytosis may possibly be responsible for the significantly enhanced uptake of Tf-conjugated nanoparticles in comparison to unconjugated NPs. These results are consistent with the findings reported by various researchers (Gan and Feng, 2010). Poor brain uptake of free Pioglitazone and Rosiglitazone may be due to their inability to permeate across the BBB and being substrates to Pgp and MDR efflux transporters, present at the blood brain barrier. The unconjugated and Tf-conjugated nanoparticles showed improved localization of the drug in the brain. The hydrophilic surface characteristic of the nanoparticles, due to the surface cross-linked PVA, could have lead to increase in the residence time in blood and thereby leading to enhanced brain deposition.

The preferential accumulation of Tf-conjugated NP's across the BBB may be the result of different events. The abundance of transferrin receptors on BBB could have resulted in the receptor mediated endocytosis, thereby transporting the nanoparticles to the brain (Skarlatos et al., 1995; Soni et al., 2005). The study clearly indicated the superiority of Tf-conjugated nanoparticles in contrast to the free drugs and unconjugated nanoparticles in increasing the accumulation of PIO and ROS within the brain. The radioactivity in brain due to nanoparticulate formulations was found to be comparatively higher at each time points as compared to free drugs. These observations showed that nanoparticulate formulations are capable of enhancing the localization of drugs in the brain. A concentration of 1.14±0.12 and 1.22±0.08%ID/g brain was obtained 1 h after intravenous administration in case of Tf-PIO-NP and Tf-ROS-NP, respectively. At 6 hrs, the brain uptake of Tf-conjugated nanoparticles was 3-fold higher than unconjugated nanoparticles. This correlation demonstrates the potential of transferrin conjugation of nanocarriers in brain targeting.

In the present study, the active targeting strategy utilizing the high expression of transferrin receptors on brain capillary endothelial cells was utilized whereby transferrin ligand conjugated nanocarriers were targeted to brain with more efficiency. It is generally thought that the blood brain barrier, constituting of the tight junction between the adjacent endothelial cells severely interrupts the movement of small molecules (Gloor et al., 2001; Huber et al., 2001; Wolburg, 2002). Therefore, the extent of organ distribution of nanoparticles is presumably dependent on their permeability through the gap of the endothelial cells.

Although the exact amount of drug transported across the BBB by the targeted nanoparticles is unclear, the higher level of radioactivity in brain tissue

in the animal group treated with Tf-conjugated nanoparticles suggests that more drug was transported into this tissue.

Order of radioactivity recovered in brain after 6 hrs of administration for various Pioglitazone formulations was Tf-PIO-NP (i.v.) > PIO-NP (i.v.) > PIO-S (intranasal) > PIO-D (oral) and in case of various Rosiglitazone formulations, it was Tf-ROS-NP (i.v.) > ROS-NP (i.v.) > ROS-S intranasal) > ROS-S (i.v.) > ROS-S (oral). The highest uptake of Tf-conjugated formulations into the brain may be attributed to presence of transferrin receptors on BBB.

Images at different time intervals after administration of nanoparticulate formulation's and free drugs are shown in scintigraphs **(Fig. 8.18 to 8.21)**. These images clearly illustrate the superiority of transferrin linked nanocarriers over uncoupled nanocarriers in drug targeting to the brain.

The nanoparticulate systems due to their ability to control the release of drugs are able to maintain the drugs concentrations in blood for longer periods in comparison to drug solution. Both types of nanoparticulate formulations lead to enhanced retention in the body, which was one of the major rationales of the neuroprotective and antidiabetic therapy.

8.6 CONCLUSION

From *in vivo* studies, it was observed that there was a prominent increase in systemic retention of drugs when they were administered in nanoparticulate formulations. Experimental observations also suggested that transferrin conjugated nanoparticles were more effectively targeted to brain than free drugs and unconjugated nanoparticles. The plasma and tissue biodistribution studies have shown higher radioactivity recovery from brain with ligand coupled nanoparticles as compared to unconjugated nanoparticles and free drugs

indicating the efficacy of transferrin conjugated carrier for brain targeting of the drugs. Therefore the results confirmed that the developed delivery systems possessed an enhanced brain targeting activity in mice and are capable of reducing systemic and hepatic toxicity induced by anti-diabetic drugs when administered for long term and may be potentially used in the treatment of neurodegenerative disorders.

This study showed the profound impact of Tf conjugation on the biodistribution of nanoparticles. At 6 hrs post injection, brain accumulation of Tf-conjugated nanoparticles was significantly enhanced compared to unconjugated nanoparticles. These targeted nanocarriers appear to be a promising drug delivery systems used in the strategy of active targeting. Because of the combination of the interesting features of nanoparticles with the site specific property of Tf, this novel nanovector is of great potential interest in the field of nanomedicine.

The results demonstrated that Tf-conjugated nanoparticles improved the circulation time of drugs in the blood and enhanced the potential for transport across the BBB relative to free drug. In addition, the targeting nanoparticles lowered the level of drugs in kidney an organ for major distribution of rosiglitazone from its I.V. solution. Thus this formulation could be also useful in reducing the cardiovascular side effects of rosiglitazone.

REFERENCES:

- Agashe, H.B., Babbar, A.K., Jain, S., Sharma, R.K., Mishra, A.K., Asthana, A., Garg, M., Dutta, T., Jain, N.K. 2007. Investigations on biodistribution of technetium-^{99m}-labeled carbohydrate-coated poly(propyleneimine) dendrimers. *Nanomed.* 3(2), 120-127.
- Gan C.W. and Feng, S.S. 2010. Transferrin-conjugated nanoparticles of Poly(lactide)-d-α-Tocopheryl polyethylene glycol succinate diblock copolymer for targeted drug delivery across the blood–brain barrier. *Biomaterials.* 31(30), 7748-7757.
- Gloor, S.M., Wachtel, M., Bolliger, M.F., Ishihara, H., Landmann, R., Frei, K., 2001. Molecular and cellular permeability control at the blood-brain barrier. *Brain Res. Rev.* 36, 258–264.
- Huber, J.D., Egleton, R.D., Davis, T.P., 2001. Molecular physiology and pathophysiology of tight junctions in the blood-brain barrier. *Trends Neurosci.* 24, 719–725.
- Illum, L. 2000. Transport of drugs from the nasal cavity to central nervous system. *Eur. J. Pharm. Sci.* 11, 1-18.
- Klibanov, A.L., Maruyama, K., Beckerleg, A.M., Torchilin, V.P., Huang, L., 1991. Activity of amphipathic poly(ethylene glycol) 5000 to prolong the circulation time of nanoparticles depends on the liposome size and is unfavorable for immunoliposome binding to target. *Biochim. Biophys. Acta.* 1062, 142–148.
- Litzinger, D.C., Buiting, A.M., van Rooijen, N., Huang, L., 1994. Effect of liposome size on the circulation time and intraorgan distribution of amphipathic poly(ethylene glycol)-containing nanoparticles. *Biochim. Biophys. Acta.* 1190, 99–107.
- Liu, S., Edwards, D.S., Barrett, J.A. 1997. ^{99m}Tc labeling of highly potent small peptides. *Bioconjug. Chem.* 8(5), 621-36.
- Love, W.G., Amos, N., Williams B.D., Kellaway, I.W. 1989. Effect of liposome surface charge on the stability of technetium (^{99m}Tc) radiolabelled liposomes. *J. Microencapsul.* 6(1), 105-113.

- Maeshiba, Y., Kiyota, Y., Yamashita, K., Yoshimura, Y., Motohashi, M., Tanayama, S. Disposition of the new antidiabetic agent pioglitazone in rats, dogs, and monkeys. *Arzneimittel-Forschung.* 1997. 47, 29–35.
- Meléndez-Alafort, L., Riondato, M., Nadali, A., Banzato, A., Camporese, D., Boccaccio, P., Uzunov, N., Rosato, A., Mazzi, U. 2006. Bioavailability of ^{99m}Tc-Ha-paclitaxel complex [^{99m}Tc-ONCOFID-P] in mice using four different administration routes. *J. Labelled Comp. Radiopharm.* 49(11), 939-50.
- Panwar, P., Singh, S., Kumar, N., Rawat, H., Mishra, A.K. 2007. Synthesis, characterization, and in vivo skeletal localization of a new ^{99m}Tc-based multidentate phosphonate chelate: 5-Amino-1,3-bis(ethylamine-(N,N dimethyl diphosphonic acid) acetamido) benzene. *Bioorg. Med. Chem.* 15(2), 1138-45.
- Pedersen, W.A. and Flynn, E.R. Insulin resistance contributes to aberrant stress responses in the Tg2576 mouse model of Alzheimer's disease. *Neurobiology of Disease.* 2004. 17, 500–506.
- Ponka, P., Lok, C.N., 1999. The transferrin receptor: role in health and disease. *Int. J. Biochem. Cell. Biol.* 31, 1111–1137.
- Qian, Z.M., Li, H., Sun, H., Ho, K., 2002. Targeted drug delivery via the transferrin receptor-mediated endocytosis pathway. *Pharmacol. Rev.* 54, 561–587.
- Reddy, L.H., Sharma, R.K., Chuttani, K., Mishra, A.K., Murthy, R.S.R. 2004. Etoposide incorporated tripalmitin nanoparticles with different surface charge: Formulation, characterization, radiolabeling and biodistribution studies. *AAPS J.* 6, 1-10.
- Reddy, L.H., Sharma, R.K., Chuttani, K., Mishra, A.K., Murthy, R.S. 2005. Influence of administration route on tumor uptake and biodistribution of etoposide loaded solid lipid nanoparticles in Dalton's lymphoma tumor bearing mice. *J.Control. Release.* 105(3), 185-98.
- Richardson, V.J, Jeyasingh, K., Jewkes R.F., Ryman B.E., Tattersall M.H. 1977. Properties of [99mTc] technetium labeled liposomes in normal and tumor bearing rats. *Biochem. Soc. Trans.* 5(1), 290-291.
- Risner, M.E., Saunders, A.M., Altman, J.F., Ormandy, G.C., Craft, S., Foley, I.M., Zvartau-Hind, M.E., Hosford, D.A., Roses, A.D. Efficacy of

rosiglitazone in a genetically defined population with mild-to-moderate Alzheimer's disease. *Pharmacogenomics J.* 2006. 6(4), 246-254.

- Saha, G.B. Fundamentals of Nuclear Pharmacy. In. Radiolabelling of compounds. Fifth Edition. 2004. Springer-Verlag New York, US. pp 86-91.
- Shenoy, V.S., Vijay, I.K., Murthy R.S. 2005. Tumour targeting: Biological factors and formulation advances in injectable lipid nanoparticles. *J. Pharm. Pharmacol.* 57(4), 411-422.
- Skarlatos, S., Yoshikawa, T., Pardridge, W.M. 1995. Transport of [125 I] transferrin through the rat blood brain barrier. *Brain Res.* 683, 161-67.
- Soni, V.S., Kohli, D.V., Jain, S.K. 2005. Transferrin-coupled liposomes as drug delivery carrier for brain targeting of 5-fluorouracil. *J. Drug Target.* 13, 245-50.
- Thakkar, H., Sharma, R.K., Mishra, A.K., Chuttani, K., Murthy, R.S.R. 2004. Efficacy of chitosan microspheres for controlled intra-articular delivery of celecoxib in inflamed joints. *J. Pharm. Pharmcol.* 56(9), 1091-1099.
- Wolburg, H., Lippoldt, A., 2002. Tight junctions of the bloodbrain barrier: development, composition and regulation. *Vascul. Pharmacol.* 38, 323–337.